CHEMISTRY
A EUROPEAN JOURNAL

DOI: 10.1002/chem.200501600

Catecholase Activity of a Copper(II) Complex with a Macrocyclic Ligand: Unraveling Catalytic Mechanisms

Iryna A. Koval,[a] Katalin Selmeczi,[b] Catherine Belle,*[b] Christian Philouze,[b] Eric Saint-Aman,[c] Isabelle Gautier-Luneau,[d] Anna Maria Schuitema,[a] Marcel van Vliet,[a] Patrick Gamez,[a] Olivier Roubeau,[e] Matthias Lüken,[f] Bernt Krebs,[f] Martin Lutz,[g] Anthony L. Spek,[g] Jean-Louis Pierre,[b] and Jan Reedijk*[a]

Abstract: We report the structure, properties and a mechanism for the catecholase activity of a tetranuclear carbonato-bridged copper(II) cluster with the macrocyclic ligand [22]pr4pz (9,22-dipropyl-1,4,9,14,17,22,27,28,29,30-decaazapentacyclo[22.2.1.1^{4,7}.1^{11,14}.1^{17,20}]triacontane-5,7(28),11(29),12,18,20(30),24(27),25-octaene). In this complex, two copper ions within a macrocyclic unit are bridged by a carbonate anion, which further connects two macrocyclic units together. Magnetic susceptibility studies have shown the existence of a ferromagnetic interaction between the two copper ions within one macrocyclic ring, and a weak antiferromagnetic interaction between the two neighboring copper ions of two different macrocyclic units. The tetranuclear complex was found to be the major compound present in solution at high concentration levels, but its dissociation into two dinuclear units occurs upon dilution. The dinuclear complex catalyzes the oxidation of 3,5-di-*tert*-butylcatechol to the respective quinone in methanol by two different pathways, one proceeding via the formation of semiquinone species with the subsequent production of dihydrogen peroxide as a byproduct, and another proceeding via the two-electron reduction of the dicopper(II) center by the substrate, with two molecules of quinone and one molecule of water generated per one catalytic cycle. The occurrence of the first pathway was, however, found to cease shortly after the beginning of the catalytic reaction. The influence of hydrogen peroxide and di-*tert*-butyl-*o*-benzoquinone on the catalytic mechanism has been investigated. The crystal structures of the free ligand and the reduced dicopper(I) complex, as well as the electrochemical properties of both the Cu^{II} and the Cu^{I} complexes are also reported.

Keywords: catechol oxidase · copper · macrocyclic ligands · reaction mechanisms · semiquinone

[a] Dr. I. A. Koval, Dr. A. M. Schuitema, M. van Vliet, Dr. P. Gamez, Prof. Dr. J. Reedijk
Leiden Institute of Chemistry, Leiden University
P.O. Box 9502, 2300 RA Leiden (The Netherlands)
Fax: (+31) 715-274-451
E-mail: reedijk@chem.leidenuniv.nl

[b] Dr. K. Selmeczi, Dr. C. Belle, Dr. C. Philouze, Prof. J.-L. Pierre
LEDSS, Equipe de Chimie Biomimétique
UMR CNRS 5616, Université J. Fourier
BP 53, 38041 Grenoble Cedex (France)
Fax: (+33) 476-514-836
E-mail: catherine.belle@ujf-grenoble.fr

[c] Prof. E. Saint-Aman
Laboratoire d'Electrochimie Organique et de Photochimie Redox
UMR CNRS 5630, Université J. Fourier
BP 53 38041 Grenoble Cedex (France)

[d] Prof. Dr. I. Gautier-Luneau
Laboratoire de Cristallographie, CNRS UPR 5031
Université Joseph Fourier, 25 avenue des Martyrs
BP 166, 38042 Grenoble Cedex 9 (France)

[e] Dr. O. Roubeau
Centre de Recherche Paul Pascal—CNRS UPR 8641
115 avenue du Dr. A. Schweitzer, 33600 Pessac (France)

[f] Dr. M. Lüken, Prof. Dr. B. Krebs
Institut für Anorganische und Analytische Chemie
der Westfälischen Wilhelms-Universität Münster
Wilhelm-Klemm-Strasse 8, 48149 Münster (Germany)

[g] Dr. M. Lutz, Prof. Dr. A. L. Spek
Bijvoet Center for Biomolecular Research, Crystal and Structural Chemistry, Utrecht University
Padualaan 8, 3584 CH Utrecht (The Netherlands)

Supporting information for this article is available on the WWW under http://www.chemeurj.org/ or from the author.

Introduction

Since the report on the crystal structure of catechol oxidase by Krebs and co-authors a few years ago,[1] the interest in model compounds of this biocatalyst, as well as for other type-3 copper enzymes (e.g., hemocyanin and tyrosinase) has taken a new turn. In particular, investigations on the substrate coordination to the copper centers,[2–4] the dioxygen activation and the subsequent reactivity of the peroxodicopper species,[5–9] and the role of a thioether linkage in a close proximity of the dicopper center,[10,11] found in catechol oxidase from *Ipomoea batatas*[1] and some hemocyanins[12,13] and tyrosinases,[14] have received a significant interest from the scientific community. Although there have been numerous reports on model complexes of catechol oxidase, detailed mechanistic studies on the catechol oxidation mechanism are unfortunately quite scarce,[15–19] and only in a few cases the mode of dioxygen reduction, for example, to dihydrogen peroxide or water, has been definitely established.[15,16,18,20–24]

The mechanism of catechol oxidation by the natural enzyme, as proposed by Krebs and co-authors,[1] can be briefly outlined as follows. The native *met* (μ-hydroxo dicopper(II)) form of the enzyme reacts stoichiometrically with one equivalent of the substrate, generating the corresponding quinone and the reduced *deoxy* (dicopper(I)) form. The latter binds dioxygen in a μ-η^2:η^2 mode, resulting in the formation of the *oxy* (peroxo-dicopper(II)) form, which then oxidizes the second equivalent of catechol to quinone with the restoration of the original *met* form of the enzyme. The binding of catechol and dioxygen to the *deoxy* form may also occur simultaneously, as can be proposed from the crystal structure of the catechol oxidase adduct with the molecule of the inhibitor thiourea.[1]

Recently, we reported the mechanism of catechol oxidation by a μ-hydroxo–dicopper(II) complex with the macrocyclic ligand [22]py4pz (Figure 1, left).[8] In this complex, a

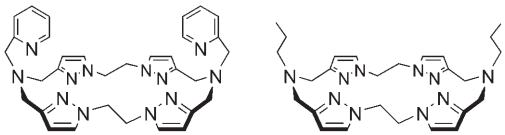

Figure 1. Schematic representation of the macrocyclic ligands [22]py4pz (left) and [22]pr4pz (right).

single hydroxo bridge connects two copper(II) ions, each of which is further coordinated by four nitrogen donor atoms, provided by the ligand. The complex oxidizes catechol by a mechanism that is rather similar to the one proposed by Krebs and co-workers.[1] Our interest in modeling the active site of the type-3 copper proteins has now prompted us to study in detail the catecholase activity of the copper(II) complex with the related macrocyclic ligand [22]pr4pz (Figure 1, right). Instead of two pyridine-containing pendant arms, present in the ligand [22]py4pz, this ligand contains two propyl residues, thus providing two N_3 donor sets for the metal coordination, and mimicking the active site of the natural enzyme even more closely. In the isolated copper(II) complex with [22]pr4pz, the two metal ions within a macrocyclic unit are bridged by a carbonate anion, and two copper ions of two different macrocyclic units are further doubly bridged by two oxygen atoms of two carbonates, resulting in a tetranuclear structure in the solid state. Herein we report on the crystal structures of the perchlorate salt of the macrocyclic ligand $[H_2[22]pr4pz](ClO_4)_2$, the tetracopper(II) complex of the composition $[Cu_2([22]pr4pz)(CO_3)(H_2O)]_2(CF_3SO_3)_4\cdot 2\,CH_3CN\cdot 4\,H_2O$ and its reduced dicopper(I) analogue $[Cu_2([22]pr4pz)(CH_3CN)_2](ClO_4)_2$, the kinetic studies on the catechol oxidation by the copper(II) complex and the anaerobic studies on its interaction with catechol, and discuss the catalytic reaction mechanism.

Results and Discussion

Synthesis of the ligand and the coordination compounds: The schematic representation of the macrocyclic ligand [22]pr4pz ((9,22-dipropyl-1,4,9,14,17,22,27,28,29,30-decaazapentacyclo[22.2.1.1^{4,7}.1^{11,14}.1^{17,20}]triacontane-5,7(28),11(29),12,18,20(30),24(27),25-octaene) is depicted in Figure 1 (right). The macrocyclic cavity comprises four pyrazolyl moieties and two nitrogen atoms of tertiary amine groups, providing two N_3 donor sets for the coordination of the metal ions. Diethyl ether diffusion into solution of copper(II) triflate (two molar equiv), the ligand (one molar equiv), and sodium carbonate (one molar equiv) in acetonitrile results in the formation of small blue crystals of the copper(II) complex. The X-ray structure determination (see below) revealed that it can be described as a tetranuclear complex of the formula $(\mathbf{I})_2(CF_3SO_3)_4\cdot 2\,CH_3CN\cdot 4\,H_2O$, in which $\mathbf{I}^{2+}$ corresponds to the dicopper unit $[Cu_2([22]pr4pz)(CO_3)(H_2O)]^{2+}$. The copper(I) complex was isolated by reacting two molar equivalents of Cu^I as a tetrakis(acetonitrile) complex with a solution of the ligand in methanol. The solid complex, which precipitated upon addition of diethyl ether, is the dinuclear Cu^I complex, denoted $\mathbf{II}(ClO_4)_2$, in which $\mathbf{II}^{2+}$ corresponds to $[Cu_2([22]pr4pz)(CH_3CN)_2]^{2+}$.

Crystal structure of $[H_2[22]pr4pz](ClO_4)_2$: The molecular structure[25] of the bis(perchlorate) salt of the ligand is shown in Figure S1 in the Supporting Information. The cationic ligand is located on an exact, crystallographic inversion center. The protonated N–H moiety acts as a donor of an intermolecular bifurcated hydrogen bond with two perchlorate oxygen atoms as acceptors; the angles at the hydrogen atom add up to 359(4)° (Table 1). Due to the inversion center in the ligand, the N21–N22 ring and its symmetry related N21′–N22′ ring are arranged in a parallel fashion; the centroid–centroid distance is 4.4089(18) Å and the parallel distance between the two planes of the aromatic rings is only 3.211 Å, indicating the presence of π stacking. The

Table 1. Bifurcated hydrogen bond for $[H_2\,[22]pr4pz](ClO_4)_2$.[a]

D–H···A	d(D–H) [Å]	d(H···A) [Å]	∢DHA [°]	d(D···A) [Å]
N27–H27···O3	0.92(3)	2.52(3)	135(2)	3.233(3)
N27–H27···O3^{i}	0.92(3)	2.25(3)	147(2)	3.063(3)

[a] Symmetry operation i: $1-x$, $-y$, $1-z$; angle O1···H27···O1^{i}: 77.2(10)°.

angle between the centroid–centroid vector and the normal to the aromatic ring plane is 43.25°.

Crystal structure of $(\mathbf{I})_2(CF_3SO_3)_4\cdot 2\,CH_3CN\cdot 4\,H_2O$: The molecular structure[25] of the isolated solid complex consists of a tetracopper complex cation $[Cu_2([22]pr4pz)(CO_3)(H_2O)]_2^{4+}$ ($(\mathbf{I})_2^{4+}$), four counter ions $CF_3SO_3^-$, two non-coordinated acetonitrile molecules, and four non-coordinated water molecules. The structure of the cation $(\mathbf{I})_2^{4+}$ is shown in Figure 2, and selected bond lengths and angles are reported in Table 2. It contains four copper(II) centers, two macrocyclic ligands, two coordinated carbonates and two coordinated water molecules. In contrast to the structure of the protonated ligand [22]pr4pz adopts a *syn* (boat) conformation, with two propyl residues located on the same side of the macrocyclic ring plane. Each macrocyclic unit encloses two copper(II) ions (Cu1 and Cu2, and Cu1′ and Cu2′), which are bridged by a carbonate anion (the Cu1···Cu2 or Cu1′···Cu2′ intramacrocyclic distance is 4.5427(18) Å). Two bridging oxygen atoms O51 and O51′ from two different carbonate molecules connect the two central copper atoms Cu1 and Cu1′ to form a centrosymmetric four-membered ring, resulting in the Cu1···Cu1′ intermacrocyclic distance of 3.281(2) Å. Each carbonate ion is thus bound in a *syn*, *syn–anti* fashion; for example, the oxygen atoms of the carbonate anion (O51 and O51′) bridge the Cu1 and Cu1′ copper atoms of two different macrocyclic rings, whereas two other oxygen atoms (O52 and O52′) bind to another copper ions (Cu2 and Cu2′, respectively).

Table 2. Selected bond lengths [Å] and angles [°] for $(\mathbf{I})_2(CF_3SO_3)_4\cdot 2\,CH_3CN\cdot 4\,H_2O$.

Cu1···Cu1′	3.281(2)	Cu1···Cu2	4.5427(18)
Cu1–O51	1.926(3)	Cu2–O52	1.957(3)
Cu1–O51′	2.330(3)	Cu2–O80	2.267(4)
Cu1–N12	2.030(5)	Cu2–N32	1.989(5)
Cu1–N17	2.025(4)	Cu2–N37	2.087(4)
Cu1–N22	2.028(5)	Cu2–N42	1.998(5)
O51-Cu1-N12	99.94(15)	O52-Cu2-O80	87.38(15)
O51-Cu1-N17	174.55(16)	O52-Cu2-N32	97.65(14)
O51-Cu1-N22	99.54(15)	O52-Cu2-N37	166.99(15)
O51-Cu1-O51′	79.47(13)	O52-Cu2-N42	96.75(14)
N12-Cu1-N17	80.9(2)	O80-Cu2-N32	96.99(16)
N12-Cu1-N22	160.18(16)	O80-Cu2-N37	105.60(16)
N12-Cu1-O51′	92.46(14)	O80-Cu2-N42	96.00(16)
N17-Cu1-N22	80.0(2)	N32-Cu2-N37	81.92(17)
N17-Cu1-O51′	95.13(14)	N32-Cu2-N42	160.99(16)
N22-Cu1-O51′	94.69(14)	N37-Cu2-N42	81.25(17)

Symmetry operation: ′ = $2-x$, y, $1/2-z$.

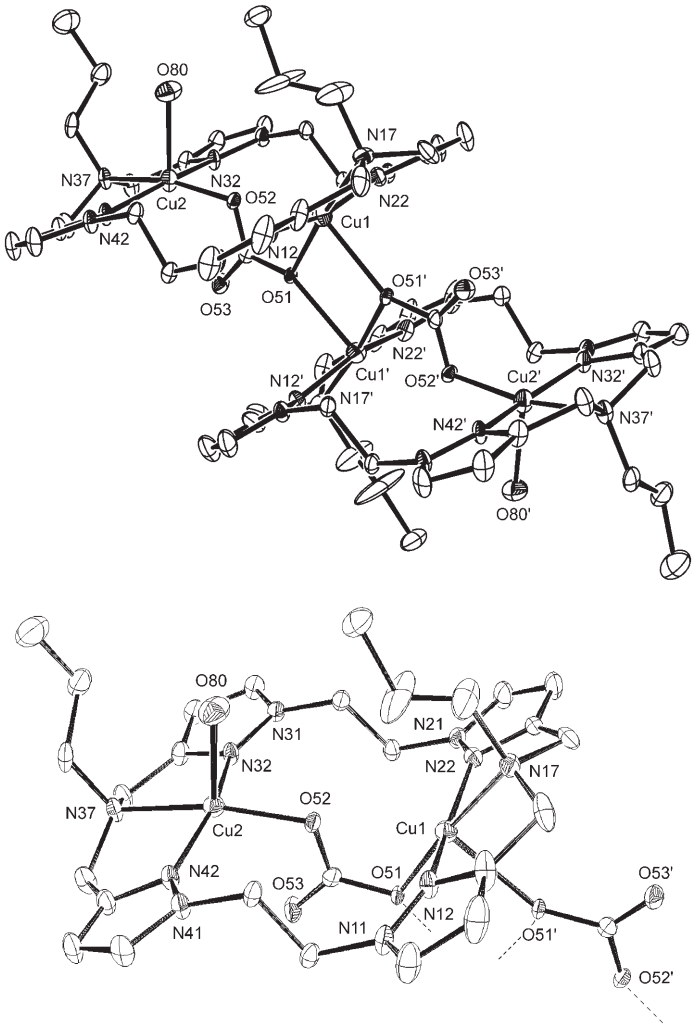

Figure 2. ORTEP projection of the tetranuclear cation $[Cu_2([22]pr4pz)(CO_3)(H_2O)]_2^{4+}$ ($(\mathbf{I})_2^{4+}$) (top) and ORTEP projection of half of the tetranuclear cation (bottom). Hydrogen atoms and solvent molecules are omitted for clarity. Symmetry operation ′: $2-x$, y, $0.5-z$.

The coordination sphere around the Cu1 ion can be described as a weakly distorted square pyramid ($\tau = 0.23$),[26] with the atoms N12, N17, N22, and O51 occupying the basal plane and the oxygen atom O51′ at a distance of 2.330(3) Å occupying the apical position. All copper–nitrogen distances are approximately equal (the average Cu1–N distance is 2.03 Å), whereas the O51 atom is located at a somewhat shorter distance of 1.926(3) Å.

Similarly, the coordination geometry around the Cu2 ion can also be best described as a weakly distorted square pyramid ($\tau = 0.1$),[26] in which the basal plane is occupied by the nitrogen atoms N32, N37, and N42 at an average distance of 2.02 Å, and the oxygen atom O52 at the distance of 1.957(3) Å. The axial position is occupied by the oxygen O80 atom from a coordinated water molecule at a distance of 2.267(4) Å.

The crystal packing was found to be uneventful, with only van der Waals interactions realized in the crystal lattice.

Crystal structure of $\mathbf{II}(ClO_4)_2$: The molecular structure of the complex cation $\mathbf{II}^{2+}$ is shown in Figure 3. Selected bond

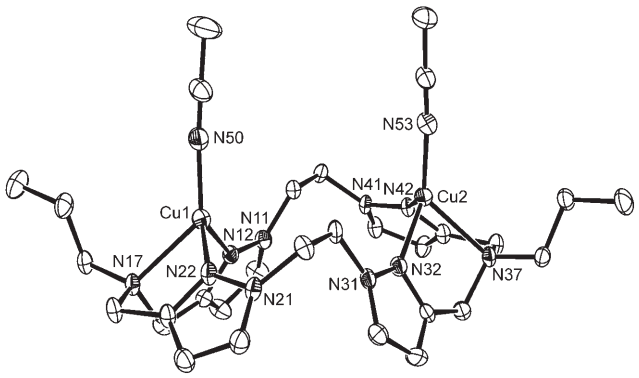

Figure 3. ORTEP projection of the complex cation $[Cu_2([22]pr4pz)(CH_3CN)_2]^{2+}$ ($\mathbf{II}^{2+}$). Hydrogen atoms are omitted for clarity.

lengths and angles are presented in Table 3. Similarly to the structure of the earlier reported dicopper(I) complex with the related macrocyclic ligand [22]py4pz, the ligand adopts a

Table 3. Selected bond lengths [Å] and angles [°] for $\mathbf{II}(ClO_4)_2$.

Cu1···Cu2	5.547(2)		
Cu1–N12	2.028(2)	Cu2–N32	2.055(2)
Cu1–N17	2.292(2)	Cu2–N37	2.277(2)
Cu1–N22	2.063(2)	Cu2–N42	2.085(2)
Cu1–N50	1.897(2)	Cu2–N53	1.903(2)
N12-Cu1-N17	79.47(8)	N32-Cu2-N37	79.64(7)
N12-Cu1-N22	112.09(8)	N32-Cu2-N42	110.05(8)
N12-Cu1-N50	121.36(9)	N32-Cu2-N53	123.26(9)
N17-Cu1-N22	78.20(8)	N37-Cu2-N42	78.06(8)
N17-Cu1-N50	131.82(8)	N37-Cu2-N53	132.19(8)
N22-Cu1-N50	121.24(9)	N42-Cu2-N53	120.69(9)

saddle-shaped conformation.[8] However, in [22]py4pz complex the tertiary nitrogen atoms of the ligand fail to bind to the metal ions, resulting in distorted trigonal surroundings for both copper(I) ions. In contrast, in $\mathbf{II}(ClO_4)_2$ both copper ions are tetracoordinate and have a distorted tetrahedral surrounding, with three positions in the coordination sphere being occupied by the nitrogen donor atoms from the ligand (N12, N17, N22 and N32, N37, N42) and one by the nitrogen atom of an acetonitrile molecule (N50 and N53). The tripodal nitrogen donor atoms N17 and N37 are located at somewhat longer distances (2.292(2) Å and 2.277(2) Å, respectively) than the nitrogen atoms of the pyrazolyl rings of the ligand (the average Cu1–$N_{pyrazole}$ distance is 2.05 Å, the average Cu2–$N_{pyrazole}$ distance is 2.07 Å). The nitrogen atoms N50 and N53 of the acetonitrile molecules are located at shorter distances of 1.897(2) Å and 1.903(2) Å, respectively. The N-Cu-N angles for both copper(I) ions vary in quite a large range, namely, from 78 to 132°, indicating a significant distortion of the coordination sphere from a regular tetrahedral geometry. The distance between the two copper(I) ions is very large, namely, 5.547(2) Å.

Magnetic properties of $(\mathbf{I})_2(CF_3SO_3)_4\cdot 2CH_3CN\cdot 4H_2O$: The thermal dependence of the complex χT (in which χ is the magnetic susceptibility per Cu_2 formula unit) is plotted in Figure 4. χT gradually increases, upon lowering the temperature, from 0.84 $cm^3 mol^{-1} K$ at 300 K to reach a maximum around 0.95 $cm^3 mol^{-1} K$ at 15 K. A decrease is then observed down to 0.81 $cm^3 mol^{-1} K$ at 5 K. Values at high temperatures are in agreement with two uncoupled spin 1/2 centers (e.g., 0.75 $cm^3 mol^{-1} K$ for $g=2$), while the increase observed is the signature of intramolecular ferromagnetic interactions. The full Hamiltonian describing the pairwise interactions among the Cu^{II} ions in $(\mathbf{I})_2(CF_3SO_3)_4\cdot 2CH_3CN\cdot 4H_2O$ can be written as Equation (1) in which the structural numbering scheme has been kept.

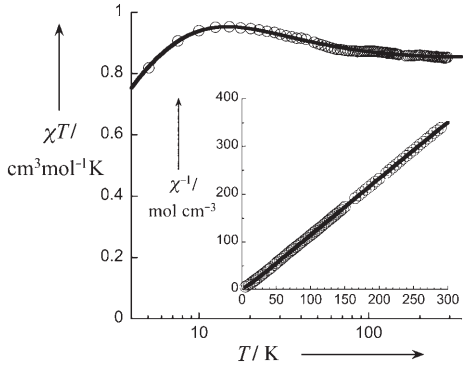

Figure 4. Semi-logarithmic plot of χT versus T for $(\mathbf{I})_2(CF_3SO_3)_4\cdot 2CH_3CN\cdot 4H_2O$ under 0.1 T applied field, in which χ is the magnetic susceptibility per Cu_2 formula unit. The inset shows the thermal dependence of the inverse magnetic susceptibility. Full lines represent the best fit obtained with a tetramer model (see text for further details).

$$H = -2J_1(S_1S_2 + S_{1'}S_{2'}) - 2J_2(S_1S_{1'}) - 2J_3(S_1S_{2'} + S_{1'}S_2) - 2J_4(S_2S_{2'}) \quad (1)$$

The energy levels and their spin quantum numbers were derived previously.[27] Testing the influence of each interaction parameter on the quality of the fit, J_4 was found to be of no influence, while J_3 was found to be undetermined when allowed to vary freely together with J_2. Indeed, although it was observed in a specific case,[27] a significant coupling between fourth neighboring spins (J_4) is unlikely. On the other hand, given the low spin density in the axial position for a close to square-pyramidal coordination environment, the central coupling pathway through the two oxygen atoms in axial and equatorial positions (J_2) can be expected to be more significant than that through the carbonato bridge also with one axial and one equatorial oxygen atom (J_3). In light of these magneto-structural considerations, J_3 and J_4 were fixed to 0. The best fit parameters were then found to be $J_1/k_B = 11.4(5)$ K, $J_2/k_B = -3.49(4)$ K and $g = 2.10(1)$, with a temperature independent paramagnetism (TIP) term of $6.6(3)\times 10^{-4}$ $cm^3 mol^{-1}$. Note that a small negative value of J_3 (<1 K) is likely, but could not be determined with accuracy, given its interdependence with J_2, and its small influence on the quality of the fit. The resulting

low-lying states are then a singlet ground state with a triplet state and a quintuplet state at about 1.4 K and 5.4 K above it, respectively. The ferromagnetic coupling propagated through the *syn–syn* carbonato bridge is in agreement with previous observations in dinuclear[28] and trinuclear[29,30] compounds with a *syn–syn* bridging coordination mode. On the other hand, because of the low spin density in axial d_{z^2} orbital, only a weak antiferromagnetic interaction, such as that found for J_2, can be expected from the orbital overlap through the asymmetric di-μ-$O_{carbonate}$ bridge.

Solution stability of $(\mathbf{I})_2(CF_3SO_3)_4\cdot 2\,CH_3CN\cdot 4\,H_2O$: ESI-MS spectra of $(\mathbf{I})_2(CF_3SO_3)_4\cdot 2\,CH_3CN\cdot 4\,H_2O$ (0.2 mM), recorded in methanol, are characterized by two peaks at $m/z = 827$ and $m/z = 1801$, which correspond to the monocharged dinuclear $[[Cu_2([22]pr4pz)(CO_3)](CF_3SO_3)]^+$ and the tetranuclear $[[Cu_2([22]pr4pz)(CO_3)]_2(CF_3SO_3)_3]^+$ ion moieties, respectively, in agreement with the theoretical isotopic patterns (Figure S2, Supporting Information). The tetranuclear copper(II) core stability in methanol and its dependence on the concentration was studied by EPR spectroscopy. The EPR spectrum of the solid sample of $(\mathbf{I})_2(CF_3SO_3)_4\cdot 2\,CH_3CN\cdot 4\,H_2O$, recorded at 13 K, is dominated by a strong isotropic signal ($g = 2.14$), which is characteristic for short-range metal–metal exchange interactions, leading to exchange narrowing. The spectrum of $(\mathbf{I})_2(CF_3SO_3)_4\cdot 2\,CH_3CN\cdot 4\,H_2O$, recorded in KBr matrix (1%), exhibits identical features (Figure 5, bold line). The spectrum of a 14 mM solution of the complex in methanol (for simplicity, the complex concentration throughout the article is calculated based on the molecular weight of the dinuclear species $[Cu_2([22]pr4pz)(CO_3)(H_2O)](CF_3SO_3)_2\cdot CH_3CN\cdot 2\,H_2O$) also contains a strong isotropic signal with the same g value; however, the typical features of a triplet spectrum, characteristic for the dinuclear copper(II) species, are also observed (Figure 5, above 0.33 T). Upon further dilution, the relative intensity of the isotropic signal gradually diminishes, until at 0.5 mM concentration, a typical triplet spectrum is finally observed. The isotropic signal, observed in the solid state is likely to be caused by the copper–copper interactions within the tetranuclear core, which also dominate in a concentrated (14 mM) solution. However, upon dilution, the dissociation of the tetranuclear cluster into two dinuclear species $\mathbf{I}^{2+}$ leads to a typical triplet dicopper(II) spectrum, which gradually increases in relative intensity on the expense of the original isotropic signal.

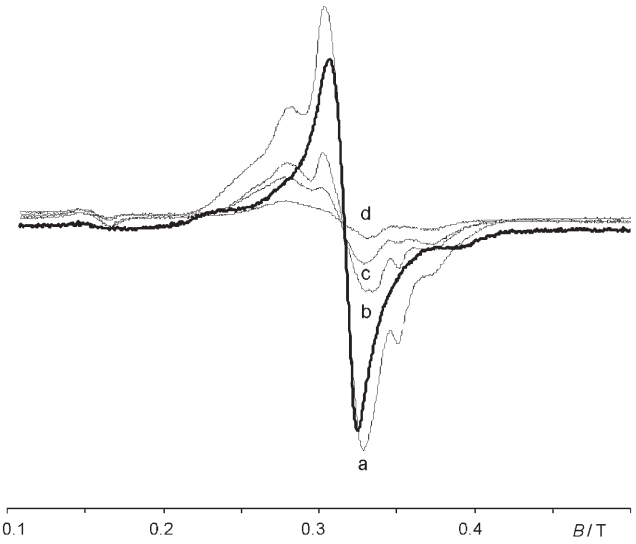

Figure 5. Bold line: EPR spectrum of $(\mathbf{I})_2(CF_3SO_3)_4\cdot 2\,CH_3CN\cdot 4\,H_2O$ in the solid state (1% in KBr matrix); solid lines: changes in the EPR spectrum of $(\mathbf{I})_2(CF_3SO_3)_4\cdot 2\,CH_3CN\cdot 4\,H_2O$ in methanol solution upon dilution (a: 14 mM, b: 2 mM, c: 1 mM, d: 0.5 mM) at 13 K.

EPR studies have also been performed on a frozen solution of the complex in acetonitrile. The spectrum practically does not change upon dilution, with the strong isotropic signal remaining dominant in the spectrum (0.4–2 mM, Figure S3, Supporting Information), suggesting that the tetranuclear core remains largely intact in this solvent.

Electrochemical properties of $(\mathbf{I})_2(CF_3SO_3)_4\cdot 2\,CH_3CN\cdot 4\,H_2O$ and $\mathbf{II}(ClO_4)_2$: The electrochemical properties of $\mathbf{I}^{2+}$ and $\mathbf{II}^{2+}$ were studied by cyclic voltammetry (CV) in methanol and in acetonitrile, using tetrabutylammonium triflate as a supporting electrolyte in case of $\mathbf{I}^{2+}$ ($NnBu_4ClO_4$ could not be used, as the complex precipitates as a perchlorate salt) and tetrabutylammonium perchlorate in case of $\mathbf{II}^{2+}$. The potentials were referred to Ag/10 mM $AgNO_3$ in acetonitrile. In the negative range of potentials, the CV curve of $\mathbf{I}^{2+}$ in MeOH (0.63 mM) is characterized by one irreversible electrochemical signal at $E_{pc} = -0.62$ V (Figure S4, Supporting Information). Coulometric titrations indicate that this peak corresponds to a one-electron transfer per copper center, resulting in the formation of Cu^I species, its re-oxidation being seen on the reverse scan as an irreversible peak at $E_{pa} = 0.14$ V. Apparently, the mixed-valence $Cu^{II}Cu^I$ species is not formed and cannot be isolated, the copper centers in $\mathbf{I}^{2+}$ being electrochemically equivalent. This result was further confirmed by following the changes in the EPR spectrum upon electrochemical reduction of the complex $\mathbf{I}^{2+}$. Since the typical triplet dicopper(II) spectrum was still observed after a one-electron transfer per dinuclear entity (Figure S5, Supporting Information)—only its intensity is decreased by a factor 2—it is concluded that no mixed-valence species could be formed.

The CV curve of $(\mathbf{I})_2(CF_3SO_3)_4\cdot 2\,CH_3CN\cdot 4\,H_2O$ in acetonitrile looks rather similar to that in methanol, with $E_{pc} = -0.72$ V and $E_{pa} = 0.18$ V. The tetranuclear core is largely preserved in the latter solvent, whereas in methanol the complex is mainly present in its dissociated form at the concentration level (0.63 mM) used for electrochemical studies; hence we can conclude that the dissociation of the dimacrocyclic unit into two dinuclear fragments does not significantly influence the metal reduction potentials.

The CV curve of $\mathbf{II}^{2+}$ in methanol is characterized by one broad electrochemical signal at $E_{pa} = 0.22$ V, that is, at a potential close to the one (0.14 V) observed for the Cu^I species electrogenerated from $\mathbf{I}^{2+}$ (Figure S6, Supporting Informa-

tion). This small difference accounts likely for small discrepancy in the coordination spheres around the copper(I) center between the two complexes, for example, caused by the initial presence of coordinated water molecules in $\mathbf{I}^{2+}$ and the acetonitrile molecule in $\mathbf{II}^{2+}$ or the carbonate bridge in the copper coordination sphere in $\mathbf{I}^{2+}$ (the carbonate bridge, however, is expected to dissociate upon electrochemical reduction due to its poor ability to bridge two copper(I) centers). Coulometric titration shows that this anodic process corresponds to a one-electron transfer per copper center leading to Cu^{II} species. The reduction of the electrogenerated two-electron-oxidized species from $\mathbf{II}^{2+}$ is seen on the CV curve, during the reverse scan, as two ill-resolved peaks at $E_{pc1}=0.03$ V and $E_{pc2}=-0.45$ V, suggesting the presence of two different electrogenerated Cu^{II} species, likely accounting for different re-coordinations with solvent molecules.

Catecholase activity of $(\mathbf{I})_2(CF_3SO_3)_4\cdot 2CH_3CN\cdot 4H_2O$—kinetic studies: The catalytic oxidation of the model substrate $DTBCH_2$ (3,5-di-*tert*-butylcatechol) by $(\mathbf{I})_2(CF_3SO_3)_4\cdot 2CH_3CN\cdot 4H_2O$ was evaluated spectrophotometrically in dioxygen-saturated methanol by monitoring the increase in absorbance at 400 nm, corresponding to the formation of the quinone product DTBQ (3,5-di-*tert*-butyl-*o*-benzoquinone). The initial reaction rates were determined from the slope of the trace at 400 nm during the first 0.7 minutes of the reaction, when the absorption at 400 nm increases linearly. Because the concentration of the complex, used for the catecholase activity studies, was 2×10^{-5} M, the active species can be regarded as dinuclear.

The rate-determining step was found to change with the substrate to complex ratio. Thus, at low substrate to complex ratios ($<$ 12:1, $[\mathbf{I}^{2+}]=2\times10^{-5}$ M), the reaction shows Michaelis–Menten behavior (Figure 6, bottom). The Lineweaver–Burk treatment gives $K_M=0.176$ mM and $V_{max}=2.47\times10^{-6}$ M s^{-1}. This behavior indicates the presence of equilibrium in the rate-determining step. At high substrate to complex ratios (up to 200:1), the reaction rate depends linearly on the $DTBCH_2$ concentration, with the first-order rate constant $k_1=2\times10^{-4}$ s^{-1} ($R^2=0.9986$, Figure 6, top).

A linear dependence on the complex concentration in the whole concentration range at all substrate to complex ratios was found (Figure 7).

The catalytic reaction was finished within a few minutes at low catechol to complex ratios, whereas at high catechol to complex ratios, full conversion of $DTBCH_2$ could not be achieved, not even after 24 h. To evaluate whether the reaction rate might be influenced by the formed product DTBQ, we performed kinetic studies in the presence of variable amounts of added quinone. DTBQ was indeed found to have a strong inhibiting effect on the catalytic process, as can be seen from Figure 8. For instance, the initial reaction rate was found to decrease to 50% of its initial value in the presence of about five molar equivalents of DTBQ. This inhibiting effect was observed both at low (10:1) and high (50:1) catechol to complex ratios ($[\mathbf{I}^{2+}]=2\times10^{-5}$ M).

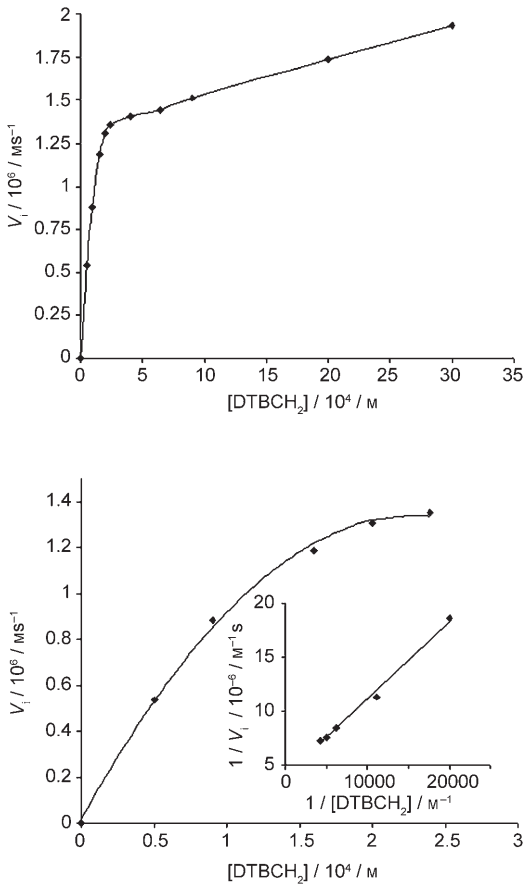

Figure 6. Top: Dependence of the initial reaction rates on catechol concentration, as determined from the slope of trace at 400 nm in the first 0.7 min of the catalytic reaction. Bottom: Dependence of the initial reaction rates on catechol concentration for substrate to catalyst ratios below 12:1 ($[\mathbf{I}^{2+}]=2\times10^{-5}$ M); the inset shows the reciprocal Lineweaver–Burk plot ($R^2=0.9932$).

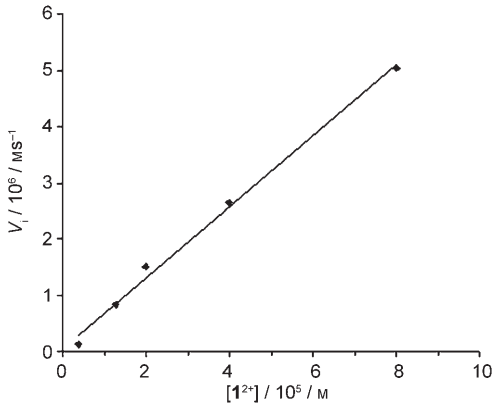

Figure 7. Dependence of the initial reaction rates on the concentration of $\mathbf{I}^{2+}$ in the catalytic oxidation of $DTBCH_2$ in methanol solution ($[DTBCH_2]=1$ mM, $k_2=0.063$ s^{-1}, $R^2=0.9945$).

Interestingly, $(\mathbf{I})_2^{4+}$ does not exhibit catecholase activity in acetonitrile. Instead, only one equivalent of quinone is formed stoichiometrically. The plot of the initial reaction rates versus catechol concentration indicates a substrate sat-

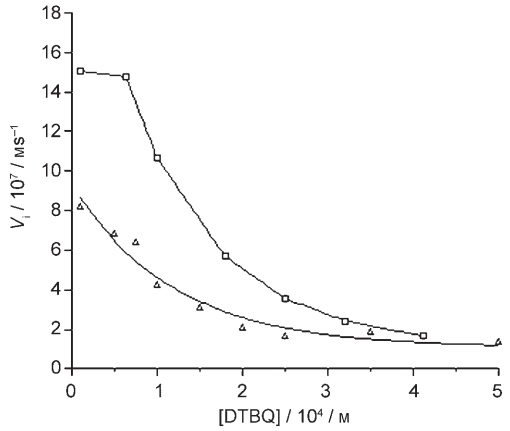

Figure 8. Dependence of the initial reaction rates on the concentration of DTBQ at low (△, 10:1) and high (□, 50:1) $DTBCH_2$ to complex ratios ($[\mathbf{I}^{2+}]=2\times10^{-5}$ M).

uration behavior (Figure S6, Supporting Information, left). The reciprocal Lineweaver–Burk plot gives $K_M=0.42$ mM and $V_{max}=5\times10^{-7}$ M s^{-1}.

Formation of H_2O_2 and its influence on the reaction: The reduction of dioxygen to dihydrogen peroxide upon catechol oxidation by copper(II) complexes has been previously established only in a few cases.[18,20–24] We have studied the formation of H_2O_2 in the course of the catalytic reaction for two different catechol to complex ratios (10:1 and 50:1, $[\mathbf{I}^{2+}]=2\times10^{-5}$ M). In both cases, dihydrogen peroxide was formed at the initial stage of the reaction, and its formation was found to practically stop after a few minutes, although the oxidation of $DTBCH_2$ still continued (Figure 9). This suggests that two different mechanisms may be operating during the catalytic oxidation of $DTBCH_2$ by $\mathbf{I}^{2+}$: one in which dioxygen undergoes a two-electron reduction to dihydrogen peroxide, and a second mechanism in which it is converted into water upon four-electron reduction.

To evaluate the influence of dihydrogen peroxide on the catalytic reaction, catalytic studies were performed in the presence of variable amounts of H_2O_2. The plot of the initial reaction rates versus dihydrogen peroxide concentrations is depicted in Figure 10. As can be seen, at low H_2O_2 concentrations its presence has virtually no influence on the reaction rates. At higher concentrations (above 20 molar equivalents of H_2O_2 per one mole of the complex), it accelerates the reaction rate. However, the concentration of dihydrogen peroxide, formed during the reaction, does not reach this level (Figure 9).

Anaerobic interaction of $\mathbf{I}^{2+}$ and $\mathbf{II}^{2+}$ with $DTBCH_2$ and DTBQ: As shown previously by Krebs and co-authors,[31] the catalytic cycle of catechol oxidase starts with the native *met* state of the enzyme, which reacts stoichiometrically with catechol to produce one equivalent of the quinone and leading to the dicopper(I) (*deoxy*) form. We studied the anaerobic interaction of $\mathbf{I}^{2+}$ with $DTBCH_2$ spectrophotometrically. Upon addition of one molar equivalent of

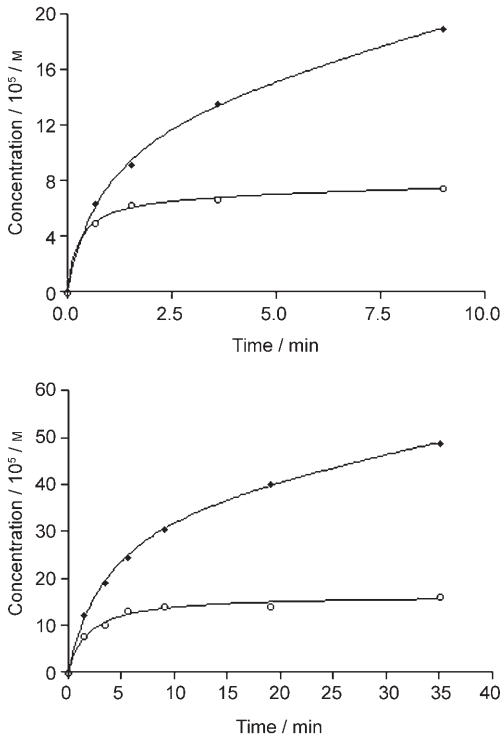

Figure 9. The course of DTBQ (◆) and H_2O_2 (○) formation during the catalytic reaction at low (10:1, top) and high (50:1, bottom) substrate to catalyst ratios ($[\mathbf{I}^{2+}]=2\times10^{-5}$ M).

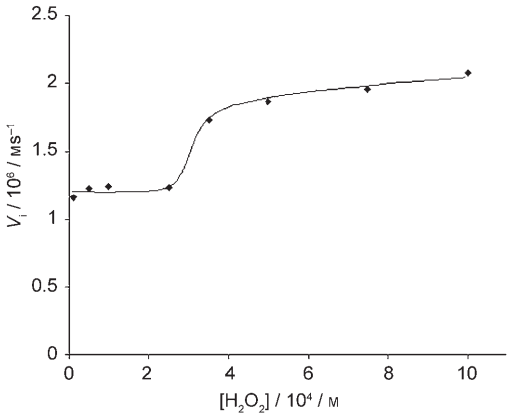

Figure 10. Dependence of the initial reaction rates in the catalytic oxidation of $DTBCH_2$ by $\mathbf{I}^{2+}$ in MeOH on the dihydrogen peroxide concentration. The initial concentration of $DTBCH_2$ is 1 mM, the concentration of $\mathbf{I}^{2+}$ is 2×10^{-5} M.

$DTBCH_2$ to a 0.5 mM solution of $\mathbf{I}^{2+}$ in methanol, two new absorptions at 389 nm ($\varepsilon=2920$ M^{-1}cm^{-1}) and 760 nm ($\varepsilon=359$ M^{-1}cm^{-1}) gradually develop in the spectrum (Figure 11, top). Both bands are characteristic of the formation of the semiquinone radical[32] and suggest that $\mathbf{I}^{2+}$ reacts with $DTBCH_2$, while undergoing a one-electron reduction, leading to the formation of mixed-valence $Cu^{II}Cu^{I}$–semiquinone species (DTSQ). The rate constant k_3 of this process is 1.8×10^{-3} M^{-1}s^{-1}. The addition of an excess of $DTBCH_2$ (up to

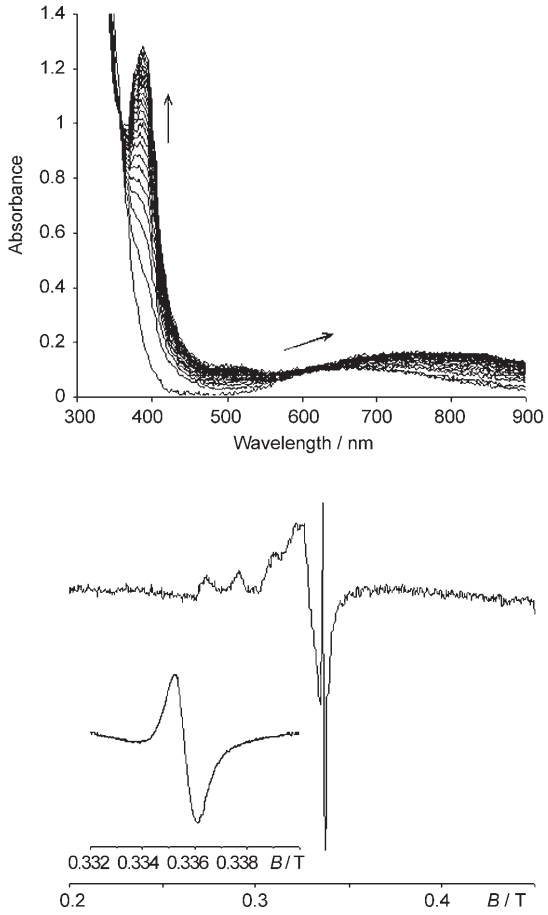

Figure 11. Top: Changes in the UV/Vis spectrum upon addition of one equivalent of $DTBCH_2$ to a solution of $\mathbf{I}^{2+}$ (0.5 mM) in methanol under anaerobic conditions at 100 K. Bottom: EPR spectrum of the resulting mixed-valence $Cu^{II}Cu^{I}$–semiquinonate species in anaerobic conditions (1 mM solution of $\mathbf{I}^{2+}$ in methanol, 100 K). Inset: the enlarged signal of the semiquinone radical.

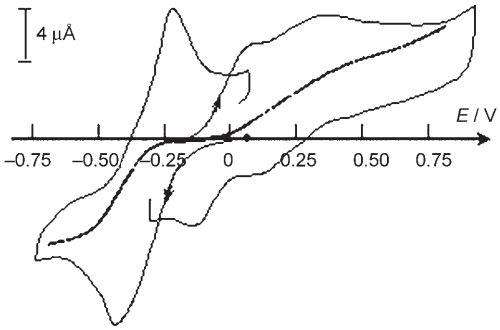

Figure 12. Electrochemical curves of $\mathbf{I}^{2+}$ (0.5 mM) in the presence of one equivalent of $DTBCH_2$, recorded under anaerobic conditions in MeOH + 0.1 M $NnBu_4CF_3SO_3$ on a C disc ($\Phi = 3$ mm). Solid line: CV curves, 0.1 $V s^{-1}$; dotted line: RDE curves, 0.01 $V s^{-1}$, $N = 600$ rpm.

five molar equivalents) has no influence on the spectrum. The formed semiquinone species is stable for at least 24 h under anaerobic conditions.

These results were further confirmed by EPR spectroscopy (Figure 11, bottom). The EPR spectrum of a 1 mM frozen solution of $\mathbf{I}^{2+}$ in the presence of one molar equivalent of $DTBCH_2$ in MeOH is characterized by a typical axial signal of mononuclear Cu^{II} species ($g_{\parallel} = 2.23$, $A_{\parallel} = 175 \times 10^{-4}$ cm^{-1}, $g_{\perp} = 2.04$) and a sharp signal centered at $g = 2.00$ corresponding to an organic radical. The results explicitly show the absence of interaction between the two metal centers, indicating the presence of discrete Cu^{II} and Cu^{I} ions within the complex, and the absence of interaction between the semiquinone radical and the Cu^{II} ion.

The electrochemical behavior of the mixed-valence $Cu^{II}Cu^{I}$–semiquinone species was also examined. The CV curve, recorded under anaerobic conditions in a 0.5 mM solution of $\mathbf{I}^{2+}$ in methanol in the presence of one molar equivalent of $DTBCH_2$ is characterized in the negative region of potentials by a reversible electrochemical signal at $E_{1/2} = -0.34$ V (Figure 12), which is followed at lower potential by the copper(0) deposition onto the electrode surface. Based on earlier reported electrochemical properties of the semiquinone species,[33,34] we have assigned this signal to the one-electron reduction of the semiquinone radical. However, a close examination of this signal shows that it displays a shoulder suggesting the presence of two overlapping electrochemical systems. It is likely that the reduction process of the Cu^{II} center in the mixed-valence $Cu^{II}Cu^{I}$–semiquinone species is hidden underneath the electrochemical response of the semiquinone moiety. In the positive range of potentials, the electrochemical curve is characterized by two ill-resolved oxidation waves at $E_{pa} = 0.12$ V and $E_{pa} = 0.42$ V (Figure 12), associated with the electrochemical responses of the $Cu^{II}Cu^{I}/Cu^{II}Cu^{II}$ redox couple and the one-electron oxidation of the semiquinone radical.

It is interesting to note that the mixed-valence $Cu^{II}Cu^{I}$ species forms readily upon anaerobic reaction of $\mathbf{I}^{2+}$ with $DTBCH_2$, whereas it could not be generated electrochemically. These results suggest an asymmetric binding of the substrate to only one of the two copper centers of the dinuclear subunit $\mathbf{I}^{2+}$ prior to the redox reaction, leading to the differentiation of the two metal centers. This in turn results in their different reduction potentials, allowing the subsequent formation of the mixed-valence dicopper core.

The mixed-valence $Cu^{II}Cu^{I}$–semiquinone species was also found to form upon treating the solution of the dicopper(I) complex $\mathbf{II}^{2+}$ (0.5 mM) with one molar equivalent of DTBQ under anaerobic conditions. In contrast to the slow reaction of $\mathbf{I}^{2+}$ with $DTBCH_2$, upon reaction of $\mathbf{II}^{2+}$ with the quinone the redox process occurs immediately, precluding the determination of the reaction rate constant. Upon exposing the resulting solution to dioxygen, the characteristic bands of semiquinone at 389 and 760 nm gradually diminish, with an isosbestic point at 460 nm, indicating its oxidation by dioxygen. Accordingly, the radical signal in the EPR spectrum disappears, and an increase of the absorption at 400 nm in the UV/Vis spectrum indicates the formation of the quinone. The iodometric H_2O_2 assay test in the presence of lactoperoxidase indicates that this process is accompanied by the formation of one equivalent of dihydrogen peroxide as a side product.

Mechanisms versus a coordination mode of the substrate: Based on the results reported above it is possible to suggest the mechanism of catechol oxidation by $\mathbf{I}^{2+}$, as depicted in Scheme 1. The catalytic cycle starts with the anaerobic oxidation of $DTBCH_2$ by $\mathbf{I}^{2+}$; however, in contrast to the natural enzyme behavior,[1,31] only one electron is transferred in the stoichiometric reaction between the complex and the substrate, leading to the formation of the mixed-valence $Cu^{II}Cu^{I}$–semiquinone species. This observation is rather interesting, as the formation of a semiquinone radical as an intermediate species in catechol oxidation was proposed earlier and/or observed in only a few cases.[23,32,35,36] In most cases, such species were formed upon reaction of catechol with mononuclear[36] or dinuclear[23] Cu^{II} complexes generated by self-assembly of two mononuclear units. In our case, however, $\mathbf{I}^{2+}$ is essentially dinuclear in solution; nevertheless, the second copper(II) ion does not participate in the redox process, playing solely a structural role.

The formed semiquinone radical is further oxidized by dioxygen, as was confirmed by UV/Vis and EPR spectroscopy. According to the earlier mechanistic reports of Kaizer et al.[36] and Kodera et al.,[23] dioxygen can bind to the Cu^{I} ion forming a Cu^{II}–superoxo species, with the consequent one-electron oxidation of the semiquinone radical leading to the release of quinone and hydrogen peroxide (Scheme 1, cycle A). However, in the course of the catalytic oxidation of $DTBCH_2$ by $\mathbf{I}^{2+}$ the concentration of H_2O_2 stops increasing after a few minutes, indicating that, most likely, a different mechanism is operating at later stages of the reaction. A proposal about H_2O_2 being consumed in the course of the reaction, as suggested by some authors,[24] does not seem plausible in this case, as the results of kinetic measurements indicate that its presence has virtually no influence on the catalytic cycle, except at unrealistically high concentrations levels, which are never reached during the reaction. Another reason to suggest a different mechanistic pathway operating at later stages of the catalytic oxidation is the inhibiting effect of DTBQ, indicating that the formed quinone does not simply accumulate in the reaction mixture, but evidently also participates in the catalytic process. This effect cannot be explained based on the simple oxidation scheme via the semiquinone formation (cycle A in Scheme 1).

Consequently, we propose that in later stages of the catalytic reaction, the oxidation of $DTBCH_2$ proceeds by a "classic" mechanism, proposed by Krebs et al.[1] and Casella et al.,[15,16] involving a stoichiometric reaction between the dicopper(II) species and the substrate, leading to the reduced dicopper(I) species. The oxidation of the second equivalent of the substrate by a peroxo–dicopper(II) adduct, formed upon dioxygen binding to the dicopper(I) intermediate, results in the formation of the second molecule of quinone and water as a by-product (Scheme 1, cycle B). The inhibiting effect of DTBQ on the catalytic cycle can then be rationalized by considering its very fast reaction with the reduced dicopper(I) species (which is the only intermediate species able to react with the quinone), leading to semiquinone formation (Scheme 1). Thus, at high concentrations, DTBQ competes with dioxygen in the reoxidation of $\mathbf{II}^{2+}$, resulting in the mixed-valence $Cu^{II}Cu^{I}$–semiquinone species, which is then subsequently oxidized in the less efficient cycle A. Consequently, the concentration of quinone increases more slowly, as only one molecule of DTBQ is produced in cycle A, in contrast to cycle B.

On the other hand, when present in high concentration (Figure 10), H_2O_2 can compete with dioxygen in the reoxidation of the dicopper(I) complex to the dicopper(II) state, therefore the increase in its concentration results in its progressive involvement as copper(I) oxidant. The increase of the reaction rates in this case can be explained by a change in the rate-determining step of the reaction, as previously proposed by Casella and co-workers.[15]

The change of the catalytic mechanism in the course of the reaction can be explained by proposing that the different mechanistic pathways are directly related to the binding mode of the substrate to the dicopper(II) core. This hypothesis has often been debated in the literature in the past years.[2–4,20,37] Up till now, different examples of substrate coordination modes to dicopper(II) complexes have been reported. Although the first example of a dicopper(II)–catecholate adduct, crystallized by Karlin,[37] showed the cate-

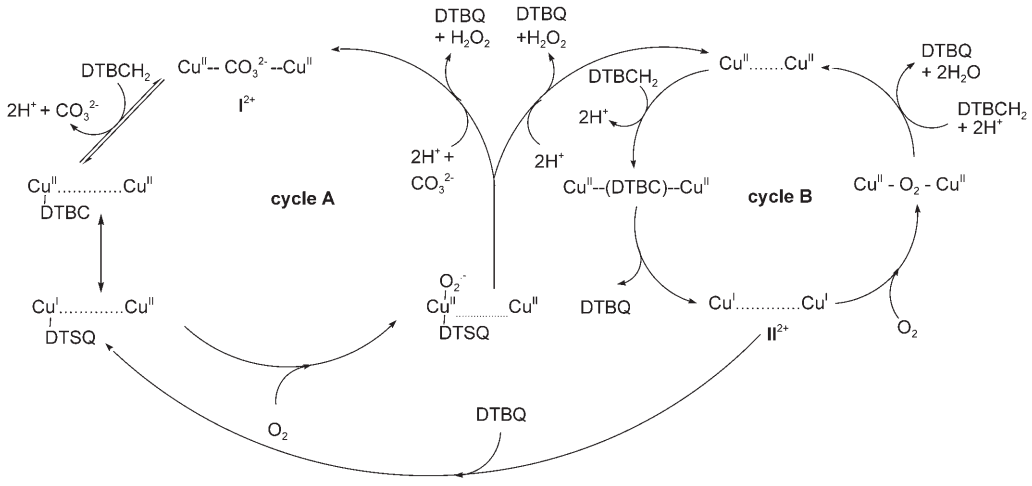

Scheme 1. The proposed mechanism for the catalytic catechol oxidation by $\mathbf{I}^{2+}$.

cholate to be coordinated as a bridging didentate ligand to both dicopper(II) centers, later reports from Casella[4] and Meyer[20] argued for an asymmetric binding of catechol to only one of the two available copper(II) ions in an η^2 fashion, possibly with one of the two oxygen atoms being involved in a weak interaction with either an adjacent copper(II) ion, or in hydrogen bonding. This apparent contradiction can be rationalized by considering that the binding mode of the substrate is, to a large extent, determined by the distance between the two copper centers and their accessibility. Thus, the short metal–metal distance promotes a binding of the catecholate in a didentate bridging fashion (e.g., in the dicopper(II)–catecholate adduct reported by Karlin[37] the two metal ions are kept at a distance of 3.248 Å), whereas in case of long metal–metal separation, a binding of the substrate to only one of the two metal centers occurs. Consequently, in the latter case, only one electron can be transferred from the substrate to the metal center, resulting in the semiquinone formation, the subsequent oxidation of which proceeds by the mechanism proposed by Kodera[23] (Scheme 1, cycle A). In the case of a didentate bridging coordination, both copper ions are reduced in the stoichiometric reaction with the substrate, leading to the quinone formation and the reduced dicopper(I) species, and the catalytic reaction further proceeds by means of the mechanism suggested by Krebs et al.[1] for the natural enzyme (Scheme 1, cycle B).

The long Cu1–Cu2 separation (4.5427(18) Å) observed for the two copper ions in the macrocyclic unit in $\mathbf{I}^{2+}$ prohibits the substrate binding in a bridging didentate fashion, thus favoring the binding of catechol to only one metal center with semiquinone formation. However, it is liable that in the course of the catalytic reaction the original dicopper(II) core undergoes substantial modification, as the carbonate bridge is likely to be cleaved by the incoming catecholate, as proposed in Scheme 1. Our earlier studies on other dicopper complexes with structurally related macrocyclic ligands[38,39] indicate that the macrocyclic cavity has a sufficient flexibility to bring two copper ions within a short distance of each other, required for a didentate bridging coordination mode of catechol. As a result, in the absence of the rigid carbonate bridge the substrate can bind to both copper(II) ions in a bridging fashion, pushing the catalytic reaction towards the cycle B, whereas the relative influence of mechanistic pathway A becomes negligible after a few minutes of the reaction.

Concluding Remarks

It is very interesting to compare the catalytic behavior of $\mathbf{I}^{2+}$ with earlier reported examples of synthetic models of catechol oxidase. The metal–metal distance in the dicopper(II) core of $\mathbf{I}^{2+}$ exceeds 4.5 Å and is thus much longer than the usual range found in catalytically active copper(II) compounds (2.9–3.5 Å). However, $\mathbf{I}^{2+}$ still exhibits catecholase activity, proving that a large copper–copper separation does not inhibit the catalytic properties. Furthermore, the results can give an answer to the question, whether the binding of the substrate to the dicopper core includes a bridging catecholate coordinated to the two copper ions[40] rather than a monodentate coordination to only one metal center,[31] demonstrating that in fact both options are possible. It is also clear that different binding modes of the substrate to a dicopper(II) core result in completely different mechanisms of catechol oxidation by dicopper(II) complexes; furthermore, in case of sufficiently flexible ligands, both mechanistic pathways can be realized.

In addition, a possible mechanism for the formation of dihydrogen peroxide is now established. Previously, it has been suggested that the formation of dihydrogen peroxide is the result of either the protonation of the peroxo–dicopper intermediate, or its reaction with catechol, leading to the formation of the reduced dicopper(I) species along with H_2O_2.[16,20,41] However, to the best of our knowledge, no actual proof that either of these pathways indeed takes place has been reported, although the formation of dihydrogen peroxide upon treating trans-μ-1,2-peroxo–dicopper(II) species with a strong acid is known.[42,43] We thus believe that dihydrogen peroxide is formed as a byproduct during the oxidation of the semiquinone intermediate with dioxygen, when the metal–metal distance within a dicopper(II) complex is too long to allow the binding of the substrate in a didentate bridging fashion. Indeed, Meyer and co-workers reported a recovery of 58–71% of dihydrogen peroxide for a series of dicopper(II) complexes,[20] for which an asymmetric coordination mode of a nonreactive catechol to only one of the copper(II) centers has been clearly established. In addition, two other crystallographically characterized dicopper(II) complexes with essentially dinucleating ligands, for which the reduction mode of dioxygen to dihydrogen peroxide has been definitely established, also possess a large metal–metal separation (3.7 Å and 7.8 Å).[18]

It thus appears that the mechanism of catechol oxidation by the model compounds is very intricate, which evidently explains often contradictory literature reports on the catalytic behavior of copper(II) complexes. It is also very interesting to note that some authors have recently reported the formation of dihydrogen peroxide,[44] as well as semiquinone radicals,[45] during the catalytic oxidation of DOPA by the structurally related enzyme tyrosinase in haemolymph of some insects. Although neither of these species has to the best of our knowledge ever been observed during the substrate oxidation by catechol oxidase, the question about the possibility of two different catechol oxidation pathways for the natural enzyme, as found for model compounds, still needs to be answered.

Experimental Section

All starting materials were commercially available and used as purchased, unless stated otherwise. The macrocyclic ligand [22]pr4pz was synthesized as previously described.[38] The single crystals of

$[H_2$ [22]pr4pz$](ClO_4)_2$ suitable for X-ray crystal structure determination were obtained by diffusion of diethyl ether into a solution containing one equivalent of [22]pr4pz and two equivalents of perchloric acid in methanol. The solution ligand-field spectra were recorded on a Varian Cary 50 Scan UV/Vis spectrophotometer and on a Zeiss MCS500 Diode-Array spectrometer ($l = 0.5$ cm). X-band electron paramagnetic resonance (EPR) measurements were performed on a Bruker ESP 300E spectrometer equipped with a Bruker nitrogen flow cryostat, or on a Bruker EMX spectrometer equipped with an ESR 900 helium flow cryostat (Oxford Instruments). The electrochemical behavior of the complexes was investigated in a 0.1 M solution of tetra-*n*-butylammonium perchlorate (TBAP) or tetra-*n*-butylammonium triflate in methanol using a EGG 273 potentionstat coupled with a Kipp & Zonen *x*–*y* recorder. The experiments were performed at room temperature in a three-compartment cell. Potentials were referred to an Ag/10 mM $AgNO_3 + CH_3CN + 0.1$ M TBAP reference electrode. The working electrode was a platinum disk of 5 mm diameter. The working electrode was polished with 1 μm diamond paste prior to each recording. C, H, N, S determinations were performed on a Perkin Elmer 2400 Series II analyzer. ESI-mass spectra in methanol or acetonitrile were recorded on a Bruker Esquire 300 apparatus.

Synthesis of $[Cu_2([22]pr4pz)(CO_3)(H_2O)]_2(CF_3SO_3)_4\cdot 2CH_3CN\cdot 4H_2O$ ($(\mathbf{I})_2(CF_3SO_3)_4\cdot 2CH_3CN\cdot 4H_2O$): Copper(II) triflate (36.9 mg, 0.10 mmol) was dissolved in acetonitrile (5 mL) and the resulting solution was added to a suspension of the ligand [22]pz4pz (25 mg, 0.05 mmol) in the same solvent (3 mL; the ligand does not dissolve, unless coordinated to the metal ions). A solution of anhydrous Na_2CO_3 (5.4 mg, 0.05 mmol) in a minimal amount of water was added to the resulting clear blue solution. The small amount of precipitate, most likely basic copper carbonate, was filtered off. Diethyl ether diffusion into the resulting greenish-blue solution led to the appearance of small blue crystals, which were found to be of a sufficient quality for X-ray single-crystal structure determination. Elemental analysis calcd (%) for $C_{62}H_{94}N_{22}O_{24}F_{12}S_4Cu_4$: C 34.8, H 4.4, N 14.4; found: C 35.1, H 4.6, N 14.4; ESI-MS in CH_3OH: *m*/*z*: 1801 $[[Cu_2([22]pr4pz)(CO_3)]_2(CF_3SO_3)_3]^+$, 827 $[[Cu_2([22]pr4pz)(CO_3)](CF_3SO_3)]^+$.

Synthesis of $[Cu_2([22]pr4pz)(CH_3CN)_2](ClO_4)_2$ ($\mathbf{II}(ClO_4)_2$): In a dry glove box, a solution of $[Cu(CH_3CN)_4]ClO_4$ (13.1 mg, 0.04 mmol) in dry methanol (2 mL) was added to a solution of [22]py4pz (9.8 mg, 0.02 mmol) in methanol (2 mL). The diffusion of diethyl ether into the resulting solution led to the appearance of very small colorless crystals, suitable for X-ray diffraction analysis. The complex was easily oxidized and could only be stored in a dry glove box atmosphere. ^{1}H NMR (CD_3OD, 300 MHz, 25 °C, TMS): $\delta = 7.72$ (d, $^3J(H,H) = 2$ Hz, 4H; 5′*H*(pz)), 6.32 (d, $^3J(H,H) = 2$ Hz, 4H; 4′*H*(pz)), 4.87 (s, 8H; pz-$(CH_2)_2$-pz), 3.65 (s, 4H; N-CH_2-pz), 2.65 (t, $^3J(H,H) = 8$ Hz, 4H; N-CH_2-C_2H_5), 1.50 (m, 4H; N-CH_2-CH_2-CH_3), 0.86 ppm (t, $^3J(H,H) = 7$ Hz, 6H; N-C_2H_5-CH_3). ESI-MS (CH_3CN) *m*/*z*: 717 $[[Cu_2([22]py4pz)]ClO_4]^+$.

X-ray crystallographic studies: X-ray intensities of $[H_2[22]pr4pz](ClO_4)_2$ were measured on Nonius KappaCCD diffractometer with rotating anode and graphite monochromator ($Mo_{K\alpha}$ radiation: $\lambda = 0.71073$ Å). The structure was solved with direct methods (SHELXS97[46]) and refined with SHELXL97[47] against F^2 of all reflections. Non-hydrogen atoms were refined freely with anisotropic displacement parameters. All hydrogen atoms were located in the difference Fourier map. The N–H hydrogen atom was refined freely with isotropic displacement parameters, C–H hydrogen atoms were refined with a riding model. Geometry calculations and checking for higher symmetry were performed with the Platon package.[25]

X-ray intensities of compound $(\mathbf{I})_2(CF_3SO_3)_4\cdot 2CH_3CN\cdot 4H_2O$ were measured on a Bruker AXS Apex diffractometer with a graphite monochromator ($Mo_{K\alpha}$ radiation: $\lambda = 0.71073$ Å). The structure was solved with direct methods (SHELXS97[46]) and the refinement was performed with SHELXL97[47] against F^2 of all reflections. Molecular illustrations, and checking for higher symmetry and geometry calculations were performed with the Platon package.[25] The hydrogen atoms of the complex cation were calculated on idealized positions using a riding model with isotropic displacement parameters. The hydrogen atoms of the co-crystallized solvent molecules were not calculated. All non-hydrogen atoms were refined anisotropically.

Due to sensitivity of $\mathbf{II}(ClO_4)_2$ towards dioxygen, the crystal was dropped into grease and then quickly frozen at 150 K on the Bruker AXS-Enraf-Nonius Kappa-CCD diffractometer using a graphite monochromator ($Mo_{K\alpha}$ radiation: $\lambda = 0.71073$ Å). The crystal was twinned and the two components were separated using the EvalCCD software package[48] with the following twin law [1 −0.65 −0.32, 0 −1 0, 0 0 −1] corresponding to a twofold axis along the [1 0 0] direction. The structure was solved by direct methods and refined by full-matrix least-squares, based on F^2 from the HKLF5 file[49] by using the SHELXL97 software[47] through the WinGX program.[50] The fractional contributions of two domains were refined and are 0.737(1), 0.263(1).

Further crystallographic data and additional parameters are given in Table 4. CCDC-290372 ($(H_2[22]pr4pz)(ClO_4)_2$), CCDC-290373 ($(\mathbf{I})_2(CF_3SO_3)_4\cdot 2CH_3CN\cdot 4H_2O$), and CCDC-284146 ($\mathbf{II}(ClO_4)_2$) contain the

Table 4. Crystallographic data for $[H_2[22]pr4pz](ClO_4)_2$, $[Cu_2([22]pr4pz)(CO_3)(H_2O)]_2(CF_3SO_3)_4\cdot 2CH_3CN\cdot 4H_2O$ and $[Cu_2([22]pr4pz)(CH_3CN)_2](ClO_4)_2$.

	$[H_2[22]pr4pz](ClO_4)_2$	$(\mathbf{I})_2(CF_3SO_3)_4\cdot 2CH_3CN\cdot 4H_2O$[a]	$\mathbf{II}(ClO_4)_2$
formula	$[C_{26}H_{40}N_{10}](ClO_4)_2$	$[Cu_4C_{54}H_{80}N_{20}O_8](CF_3SO_3)_4\cdot 2CH_3CN\cdot 4H_2O$	$[Cu_2C_{30}H_{44}N_{12}](ClO_4)_2$
M_r	691.58	2123.85	898.75
crystal system	monoclinic	monoclinic	triclinic
space group	$P2_1/c$ (no. 14)	$C2/c$ (no. 15)	$P\bar{1}$ (no. 2)
a [Å]	8.0611(14)	18.716(5)	11.079(3)
b [Å]	11.660(2)	15.043(5)	11.825(4)
c [Å]	17.306(3)	32.110(5)	17.329(5)
α [°]	90	90	87.10(2)
β [°]	96.557(16)	103.118(5)	74.92(2)
γ [°]	90	90	68.81(2)
V [Å^3]	1615.9(5)	8804(4)	2041.5(11)
Z	2	4	2
ρ_{calcd} [g cm^{-3}]	1.421	1.602	1.462
$F(000)$	728	4328	928
μ [mm^{-1}]	0.264	1.156	1.233
crystal color	colorless/yellowish	blue	colorless
T [K]	150	153	150
θ min/max [°]	2.1/25.5	1.3/25.9	1.22/30.11
reflns measured	23591	25022	38986
independent reflns (R_{int})	3002 (0.063)	8021 (0.177)	10797
observed reflns [$I > 2\sigma(I)$]	2353	4805	30714
parameters/restraints	213/0	597/0	0
$R1$ [$I > 2\sigma(I)$]	0.0529	0.0705	0.0591
$wR2$ (all data)	0.1415	0.2007	0.1632
S	1.06	0.94	1.07
min/max residual density [e Å^{-3}]	−0.59/0.42	−1.33/1.41	−1.81/1.40

[a] The entries for formula weight, density, $F(000)$ and μ of complex $(\mathbf{I})_2(CF_3SO_3)_4\cdot 2CH_3CN\cdot 4H_2O$ are based on the formula $C_{54}H_{76}Cu_4N_{20}O_8(CF_3O_3S)_4\cdot 2(C_2N)\cdot 4(O)$, which does not contain the hydrogen atoms of the solvent molecules.

supplementary crystallographic data for this paper. These data can be obtained free of charge from The Cambridge Crystallographic Data Centre via www.ccdc.cam.ac.uk/data_request/cif.

Catecholase activity studies: The catecholase activity of $\mathbf{I}^{2+}$ was evaluated by reaction with 3,5-di-*tert*-butylcatechol at 25 °C in methanol. The absorption at 400 nm ($\varepsilon = 1400\,\text{M}^{-1}\text{cm}^{-1}$), characteristic of the formed quinone, was measured as a function of time. The experiments were run under 1 atm of dioxygen. The kinetic parameters were determined for 2×10^{-5} M solutions of the complex (for simplicity, the complex concentration throughout the article has been calculated based on the molecular weight of dinuclear species $([Cu_2([22]pr4pz)(CO_3)(H_2O)](CF_3SO_3)_2\cdot CH_3CN\cdot 2H_2O$) and 0.05–3 mM solutions of the substrate. In a typical catalytic experiment, 2.5 mL of the solution of $\mathbf{I}^{2+}$ were placed in a 1 cm path-length cell, and the solution was saturated with dioxygen. Afterwards, 75 μL of the solution of substrate were added. After thorough shaking, the changes in UV/Vis spectra were recorded over a period of 30 min.

Effect of dihydrogen peroxide on the kinetics of $DTBCH_2$ oxidation: The effect of dihydrogen peroxide on the reaction rates was studied in dioxygen-saturated methanol by varying the concentration of H_2O_2 in the range of 0.01–1 mM at constant concentrations of the complex (2×10^{-5} M) and $DTBCH_2$ (1 mM).

Effect of 3,5-DTBQ on the kinetics of $DTBCH_2$ oxidation: The effect of DTBQ on the reaction rates was studied in dioxygen-saturated methanol by varying the concentration of DTBQ in the range of 0.01–0.412 mM at constant concentrations of the complex and $DTBCH_2$. The concentration of $\mathbf{I}^{2+}$ was 2×10^{-5} M; the concentration of $DTBCH_2$ was 0.2 mM and 1 mM.

Detection of dihydrogen peroxide in the catalytic $DTBCH_2$ oxidation: The presence of dihydrogen peroxide in the reaction mixture was analyzed using the iodiometric assay based on I_3^-, which has a characteristic absorption band at 353 nm ($\varepsilon = 26000\,\text{M}^{-1}\text{cm}^{-1}$ in water). The oxidation reaction of $DTBCH_2$ by $\mathbf{I}^{2+}$ was carried out as described in the kinetic experiment. When the formation of quinone reached a desired value at 400 nm the solution was acidified with H_2SO_4 to pH 2 to stop the reaction. Water (3 mL) was added and the reaction mixture was then extracted with CH_2Cl_2 (×2) to remove the formed DTBQ. A solution of KI (1 mL, 0.3 M) in water with a catalytic amount of lactoperoxidase, to accelerate the formation of I_3^-, was added to a 2 mL aliquot of the aqueous layer. Blank experiments were performed under identical conditions in the presence of DTBQ and $\mathbf{I}^{2+}$, but only minor formation of I_3^- was observed.

Acknowledgements

Support of the NRSC Catalysis (a Research School Combination of HRSMC and NIOK) is kindly acknowledged. Also support and sponsorship concerted by COST Action D21/003/2001 is gratefully acknowledged. Collaborative travel grant from the French Ministry of Research and Foreign Affairs (EGIDE) and NWO (Van Gogh Programme and CW: M.L. and A.L.S.), allowing visits and exchanges between Leiden and Grenoble, is gratefully acknowledged. The work was in part supported by CNRS/DFG program with a grant for K.S. The authors thank the Institute of Metals in Biology of Grenoble that provided the facilities for performing 13 K EPR, and Dr. Stéphane Ménage for assistance in these experiments.

[1] T. Klabunde, C. Eicken, J. C. Sacchettini, B. Krebs, *Nat. Struct. Biol.* **1998**, *5*, 1084–1090.
[2] S. Torelli, C. Belle, S. Hamman, J. L. Pierre, E. Saint-Aman, *Inorg. Chem.* **2002**, *41*, 3983–3989.
[3] H. Börzel, P. Comba, H. Pritzkow, *Chem. Commun.* **2001**, 97–98.
[4] T. Plenge, R. Dillinger, L. Santagostini, L. Casella, F. Tuczek, *Z. Anorg. Allg. Chem.* **2003**, *629*, 2258–2265.
[5] L. M. Berreau, S. Mahapatra, J. A. Halfen, R. P. Houser, V. G. Young, W. B. Tolman, *Angew. Chem.* **1999**, *111*, 180–183; *Angew. Chem. Int. Ed.* **1999**, *38*, 207–210.
[6] V. Mahadevan, L. Dubois, B. Hedman, K. O. Hodgson, T. D. Stack, *J. Am. Chem. Soc.* **1999**, *121*, 5583–5584.
[7] L. Santagostini, M. Gulotti, E. Monzani, L. Casella, R. Dillinger, F. Tuczek, *Chem. Eur. J.* **2000**, *6*, 519–522.
[8] I. A. Koval, C. Belle, K. Selmeczi, C. Philouze, E. Saint-Aman, A. M. Schuitema, P. Gamez, J.-L. Pierre, J. Reedijk, *J. Biol. Inorg. Chem.* **2005**, *10*, 739–750.
[9] L. M. Mirica, M. Vance, D. J. Rudd, B. Hedman, K. O. Hodgson, E. I. Solomon, T. D. P. Stack, *Science* **2005**, *308*, 1890–1892.
[10] I. A. Koval, M. Huisman, A. F. Stassen, P. Gamez, O. Roubeau, C. Belle, J. L. Pierre, E. Saint-Aman, M. Luken, B. Krebs, M. Lutz, A. L. Spek, J. Reedijk, *Eur. J. Inorg. Chem.* **2004**, 4036–4045.
[11] M. Merkel, N. Möller, M. Piacenza, S. Grimme, A. Rompel, B. Krebs, *Chem. Eur. J.* **2005**, *11*, 1201–1209.
[12] M. E. Cuff, K. I. Miller, K. E. van Holde, W. A. Hendrickson, *J. Mol. Biol.* **1998**, *278*, 855–870.
[13] C. Gielens, N. de Geest, X. Q. Xin, B. Devreese, J. van Beeumen, G. Preaux, *Eur. J. Biochem.* **1997**, *248*, 879–888.
[14] K. Lerch, *J. Biol. Chem.* **1982**, *257*, 6414–6419.
[15] E. Monzani, L. Quinti, A. Perotti, L. Casella, M. Gulotti, L. Randaccio, S. Geremia, G. Nardin, P. Faleschini, G. Tabbi, *Inorg. Chem.* **1998**, *37*, 553–562.
[16] E. Monzani, G. Battaini, A. Perotti, L. Casella, M. Gullotti, L. Santagostini, G. Nardin, L. Randaccio, S. Geremia, P. Zanello, G. Opromolla, *Inorg. Chem.* **1999**, *38*, 5359–5369.
[17] K. Selmeczi, M. Reglier, G. Speier, G. Peintler, *React. Kinet. Catal. Lett.* **2004**, *81*, 143–151.
[18] K. Selmeczi, M. Reglier, M. Giorgi, G. Speier, *Coord. Chem. Rev.* **2003**, *245*, 191–201.
[19] A. Granata, E. Monzani, L. Casella, *J. Biol. Inorg. Chem.* **2004**, *9*, 903–913.
[20] J. Ackermann, F. Meyer, E. Kaifer, H. Pritzkow, *Chem. Eur. J.* **2002**, *8*, 247–258.
[21] J. Balla, T. Kiss, R. F. Jameson, *Inorg. Chem.* **1992**, *31*, 58–62.
[22] J.-P. Chyn, F. L. Urbach, *Inorg. Chim. Acta* **1991**, *189*, 157–163.
[23] M. Kodera, T. Kawata, K. Kano, Y. Tachi, S. Itoh, S. Kojo, *Bull. Chem. Soc. Jpn.* **2003**, *76*, 1957–1964.
[24] A. Neves, L. M. Rossi, A. J. Bortoluzzi, B. Szpoganicz, C. Wiezbicki, E. Schwingel, W. Haase, S. Ostrovsky, *Inorg. Chem.* **2002**, *41*, 1788–1794.
[25] A. L. Spek, *J. Appl. Crystallogr.* **2003**, *36*, 7–13.
[26] A. W. Addison, T. N. Rao, J. Reedijk, J. van Rijn, G. C. Verschoor, *J. Chem. Soc. Dalton Trans.* **1984**, 1349–1356.
[27] B. Chiari, O. Piovesana, T. Tarantelli, P. F. Zanazzi, *Inorg. Chem.* **1993**, *32*, 4834–4838.
[28] A. L. van den Brenk, K. A. Byriel, D. P. Fairlie, L. R. Gahan, G. R. Hanson, C. J. Hawkins, A. Jones, C. H. L. Kennard, B. Moubaraki, K. S. Murray, *Inorg. Chem.* **1994**, *33*, 3549–3557.
[29] G. A. van Albada, I. Mutikainen, O. Roubeau, U. Turpeinen, J. Reedijk, *Inorg. Chim. Acta* **2002**, *331*, 208–215.
[30] G. A. van Albada, I. Mutikainen, O. S. Roubeau, U. Turpeinen, J. Reedijk, *Eur. J. Inorg. Chem.* **2000**, 2179–2184.
[31] C. Eicken, B. Krebs, J. C. Sacchettini, *Curr. Opin. Struct. Biol.* **1999**, *9*, 677–683.
[32] J. S. Thompson, J. C. Calabrese, *Inorg. Chem.* **1985**, *24*, 3167–3171.
[33] C. Benelli, A. Dei, D. Gatteschi, L. Pardi, *Inorg. Chem.* **1990**, *29*, 3409–3415.
[34] M. D. Stallings, M. M. Morrison, D. T. Sawyer, *Inorg. Chem.* **1981**, *20*, 2655–2660.
[35] J. S. Thompson, J. C. Calabrese, *J. Am. Chem. Soc.* **1986**, *108*, 1903–1907.
[36] J. Kaizer, J. Pap, G. Speier, L. Parkanyi, L. Korecz, A. Rockenbauer, *J. Inorg. Biochem.* **2002**, *91*, 190–198.
[37] K. D. Karlin, Y. Gultneh, T. Nicholson, J. Zubieta, *Inorg. Chem.* **1985**, *24*, 3725–3727.

[38] A. M. Schuitema, P. G. Aubel, I. A. Koval, M. Engelen, W. L. Driessen, J. Reedijk, M. Lutz, A. L. Spek, *Inorg. Chim. Acta* **2003**, *355*, 374–385.
[39] I. A. Koval, K. van der Schilden, A. M. Schuitema, P. Gamez, C. Belle, J.-L. Pierre, M. Luken, B. Krebs, O. Roubeau, J. Reedijk, *Inorg. Chem.* **2005**, *44*, 4372–4382.
[40] E. I. Solomon, U. M. Sundaram, T. E. Machonkin, *Chem. Rev.* **1996**, *96*, 2563–2605.
[41] E. Monzani, L. Casella, G. Zoppellaro, M. Gullotti, R. Pagliarin, R. Bonomo, G. Tabbi, G. Nardin, L. Randaccio, *Inorg. Chim. Acta* **1998**, *282*, 180–192.
[42] K. D. Karlin, P. Ghosh, R. W. Cruse, G. J. Meyer, A. Farooq, Y. Gultneh, R. R. Jacobson, N. J. Blackburn, R. W. Strange, J. Zubieta, *J. Am. Chem. Soc.* **1988**, *110*, 6769–6780.
[43] P. P. Paul, Z. Tyeklár, R. R. Jacobson, K. D. Karlin, *J. Am. Chem. Soc.* **1991**, *113*, 5322–5332.
[44] D. A. Komarov, I. A. Slepneva, V. V. Glupov, V. V. Khramtsov, *Free Radical Res.* **2005**, *39*, 853–858.
[45] I. A. Slepneva, D. A. Komarov, V. V. Glupov, V. V. Serebrov, V. V. Khramtsov, *Biochem. Biophys. Res. Commun.* **2003**, *300*, 188–191.
[46] G. M. Sheldrick, SHELXS-97, Program for crystal structure solution, **1997**, University of Göttingen (Germany).
[47] G. M. Sheldrick, SHELXL-97, Program for the refinement of crystal structures, **1997**, University of Göttingen (Germany).
[48] A. J. M. Duisenberg, L. M. J. Kroon-Batenburg, A. M. M. Schreurs, *J. Appl. Crystallogr.* **2003**, *36*, 220–229.
[49] R. Herbst-Irmer, G. M. Sheldrick, *Acta Crystallogr. Sect. B* **1998**, *54*, 443–449.
[50] L. J. Farrugia, *J. Appl. Crystallogr.* **1999**, *32*, 837–838.

Received: December 21, 2005
Published online: July 10, 2006

